Barrier-Free Duct Muffler For Low-Frequency Sound Absorption

Cong Gao
Hong Kong University of Science and Technology
Chuandeng Hu
Shenzhen Fantwave Tech. Co., Ltd
Jun Mei
South China University of Technology
Bo Hou
Soochow University
Xianli Zhang
Shenzhen Fantwave Tech. Co., Ltd
Zhanhang Du
South China University of Technology
Weijia Wen (phwen@ust.hk)
Hong Kong University of Science and Technology

Research Article

Keywords: Helmholtz resonator, duct muffler, ventilation sound absorption

Posted Date: March 9th, 2022

DOI: https://doi.org/10.21203/rs.3.rs-1407057/v1

Barrier-free duct muffler for low-frequency sound absorption

Cong Gao[1], Chuandeng Hu[2,*], Jun Mei[3,*], Bo Hou[4], Xianli Zhang[2], Zhanhang Du[3], Weijia Wen[1,*]

[1] Advanced Materials Thrust, Function Hub, Hong Kong University of Science and Technology, Guangzhou 511458, China
[2] Shenzhen Fantwave Tech. Co., Ltd, Shenzhen 518110, China
[3] School of Physics, South China University of Technology, Guangzhou 516040, China
[4] School of Physical Science and Technology & Collaborative Innovation Center of Suzhou Nano Science and Technology, Soochow University, Suzhou 215006, China

Correspondence and requests for materials should be addressed to:
C.H.(boson@fantwave.com), J.M.(phjunmei@scut.edu.cn) and W.W.(phwen@ust.hk)

ABSTRACT

We demonstrate a duct muffler design operating at frequency range that lower than 2000Hz. The device is composed of coupled annular Helmholtz Resonators (HRs) and installed as side branch of a circular ventilation tube to avoid affecting the ventilation. Porous material is employed for the purpose of generating asymmetric intrinsic loss status of the HR. Analytical model based on temporal coupled-mode theory is introduced and numerical simulation technique for structure design are introduced and verified. Experimental study verifies the effectiveness of the design methodology and illustrate that the device can achieve near perfect sound absorption in the desired frequency range. A symmetry configuration of HRs also experimentally proved to be able to conduct sound absorption for sound incident from both sides of the duct. This work provides a solid foundation for the application of the designed muffler and an analytical explanation of the corresponding sound absorption mechanisms.

Keywords: Helmholtz resonator, duct muffler, ventilation sound absorption

Introduction

The absorption and isolation of acoustic waves has been a challenging topic for both the engineering and academic fields because of their strong penetration capability granted by the long wavelength. The emergence of acoustic phononic crystals (APC) brought a pathway of acoustic wave manipulation through the Bragg scattering caused by the artificially designed periodic structure[1,2]. The APC can therefore form unique band structures that attenuate or encourage the propagation of corresponding acoustic waves. However, large device scale was required for low frequency waves since the lattice constant should be in the same scale as the manipulated wavelength[3]. In recent decade, acoustic metamaterials (AMMs) that can generate bandgaps based on the local resonant phenomenon is considered as a promising solution for sound absorption in the low frequency regime [4-6]. The lattice constant of the AMMs can be deep subwavelength because of the local resonance mechanism and therefore reveals obvious advantages in the low frequency acoustic field [7]. Various AMMS structures have been proposed to achieve acoustic wave manipulation or absorption function, including Helmholtz resonator (HR) [8-10], membrane-type acoustic metamaterial (MAM) [11-13], metasurface [14-16] and acoustic black hole (ABH)[17-19].

Different sound absorbers are investigated to achieve perfect absorption (PA) of sound waves propagating in diverse situations. The satisfaction of critical coupling mechanism, in which the absorber impedance matched with the impedance of the surrounding medium, is a compulsory condition for achieving maximum absorption performance [20,21]. However, earlier research work pointed out that a single absorber can only achieve 50% absorption even if with critical coupling mechanism satisfied [22]. To break such limitation, several types of solutions are proposed and investigated. The first one is to equip ancillary reflectors for absorbers [23,24]. The wave passing the absorber is reflected to the absorbers repeatedly so it can achieve near PA. However, the utilisation of reflector will also block the flow of fluid, such as air and water, and therefore make it unpractical for some application, especially under ventilation condition. To avoid the usage of reflector and to allow ventilation, the second solution is by using coherent perfect absorption (CPA) mechanism [25]. It requires an extra incident wave with properties precisely and dynamically controlled as the counterpart of incident wave [26]. But fulfilment of such requirement in application is critical since it requires extra wave generating and detecting system.

The usage of Fabry-Perot resonators (FPRs) is another solution that proposed to conduct sound absorption in ventilation condition [20]. FPRs usually use the coiling-up channels for dissipating the incident acoustic wave energy through visco-thermal effect at air-channel wall interface[27]. For example, Kumar and Lee [28] introduced a labyrinthine acoustic metastructure that can conduct broad sound absorption under ventilation condition. In addition, the usage of degenerate resonators is also proved to be effective in the ventilation sound absorption. The scattering cancellation of monopole and dipole modes leads to the total absorption of incident acoustic waves[29]. According to such

mechanism, Yang *et al* [30] presented a MAM with degenerate resonators that capable of absorbing sound incident from both sides of a duct. Similarly, Wu *et al* [22] designed a ventilated absorber, which comprised of two weakly coupled tube resonators, can perfectly absorb low frequency (<400Hz) sound incident from both sides of a duct. An ultra-open design proposed by Xiang *et al* [31]can maintain good ventilation whilst achieving sound absorption. The operation frequency can also be customized by stacking units with different geometry dimensions. However, the abovementioned designs require the absorber structure to inserted within the duct, so they will change the cross-section configuration and thus affect the ventilation status.

Detuned HR pairs equipped as duct branches is found capable of achieving near PA whilst without hindering the ventilation[32]. The HR pairs for PA consist of a highly dissipative resonator, or so-called absorber, and a reflector. The reflector, whose impedance is much less than the surrounding medium impedance, is equivalent to a soft acoustic boundary and thus preventing the wave from transmitting by reflecting the incident wave. Long *et al* [33] proposed HR designs with weak damping and high dissipation respectively by carefully adjusting the dimension of cavity and neck of the HRs. Another approach of tuning the dissipation is to employ porous materials. Lee *et al* [34] introduced an annular HR pair that can achieve near PA in duct. To increase intrinsic loss, the absorber in the upstream (near incident side) is applied with porous material at the neck area, where the wave energy is concentrated. Meanwhile, the downstream one is maintained highly reflective. Such design make the HR pair have highly asymmetric intrinsic losses and thus achieving efficient sound absorption.

However, these HR designs require accurate geometry parameter selection or precise manufacturing process to fulfil the asymmetric intrinsic losses conditions. Consequently, the continuous operation frequency tuning is difficult to realise. In addition, even though the previously mentioned study has utilised porous material as a design factor to tune the intrinsic loss of the HR[23,34], the effect of combining porous material with HR structures is not fully investigated.

In this work, we introduce a design of duct muffler that can achieve near perfect absorption (>90%) in duct system, whilst avoiding hindering the ventilation. Porous material is introduced into one of the muffler cavities and the impedance matching/mismatching is formed. Detailed porous material properties are indicated. Analytical model for the designed HR structures is developed based on the temperal coupled-mode theory (TCMT). The degeneracy of the two HRs and the corresponding acoustic wave counteracting performance can be effectively depicted by the coupled mode. The structure can also be adjusted to achieve sound absorption for wave incident from both sides. The insertion of porous material decreases the requirement for accuracy in the geometry parameters selection and allows continuous operation frequency adjustment.

Theoretical model and structure design

To illustrate the physical mechanism of the coupled HR muffler, we depict the structure by TCMT model. The configuration and physical model of the designed muffler is illustrated in Figure 1.

For simplification, only the fundamental resonance of the HR is considered, so there are two modes that coupling with the duct: the absorption φ_A and reflection φ_R. The resonators are side-coupled with the duct. The distance between the two resonators $L = \frac{\lambda}{4}$ is compulsory, where λ is the corresponding wavelength of resonant frequency, so the direct coupling between the two modes can be assumed weak. The coupling equations can then be described as:

$$\begin{cases} \frac{d\varphi_A}{dt} = \left(i\omega_A - \frac{1}{\tau_{0A}} - \frac{1}{\tau_{eA}}\right)\varphi_A + \sqrt{\frac{1}{\tau_{eA1}}}s_{1+} + \sqrt{\frac{1}{\tau_{eA2}}}s_{2+} & (1) \\ \frac{d\varphi_R}{dt} = \left(i\omega_R - \frac{1}{\tau_{0R}} - \frac{1}{\tau_{eR}}\right)\varphi_R + \sqrt{\frac{1}{\tau_{eR1}}}s_{3+} + \sqrt{\frac{1}{\tau_{eR2}}}s_{4+} & (2) \end{cases}$$

$$\begin{cases} s_{1-} = s_{2+} - \sqrt{\frac{1}{\tau_{eA2}}}\varphi_A & (3) \\ s_{2-} = s_{1+} - \sqrt{\frac{1}{\tau_{eA1}}}\varphi_A & (4) \end{cases} \qquad \begin{cases} s_{3-} = s_{4+} - \sqrt{\frac{1}{\tau_{eR2}}}\varphi_R & (5) \\ s_{4-} = s_{3+} - \sqrt{\frac{1}{\tau_{eR1}}}\varphi_R & (6) \end{cases}$$

, where s_{i+} and s_{i-} $(i = 1,2,3,4)$ are the amplitudes of incoming and outgoing waves of the resonators, ω_A and ω_R are the resonant frequencies of the absorber and reflector respectively. $\frac{1}{\tau_0}$ and $\frac{1}{\tau_e}$ are the intrinsic loss and leakage rate of the resonator. For side coupling, one can have $\frac{1}{\tau_{e1}} + \frac{1}{\tau_{e2}} = \frac{2}{\tau_e}$ [35]. The subscript j $(j = 1,2)$ of $\frac{1}{\tau_{ej}}$ represents the leakage towards left and right side of the duct. The coupling between waves and the resonant modes are merely related with the leakage rate of resonator, therefore the coupling parameter is given as $\sqrt{\frac{1}{\tau_{ei}}}$ [35]. Define $s_{4+} = 0$ for a single side incident.

In addition, because the distance between the two resonators is not negligible, a phase difference exists between the outgoing (incoming) wave of absorber and incoming (outgoing) wave of reflector. According to the transfer matrix method utilized in common acoustic wave guide, the relation can be described as[36]:

$$\begin{cases} s_{2-} = s_{3+}e^{ikl} & (7) \\ s_{2+} = s_{3-}e^{-ikl} & (8) \end{cases}$$

, where $k = \frac{2\pi}{\lambda}$.

From equation (1) and (2), according to TCMT[35], one can derive:

$$\begin{cases} \varphi_A = \frac{\sqrt{\frac{1}{\tau_{eA}}}(s_{1+}+s_{2+})}{i(\omega-\omega_A)+\frac{1}{\tau_{0A}}+\frac{1}{\tau_{eA}}} & (9) \\ \varphi_R = \frac{\sqrt{\frac{1}{\tau_{eR}}}(s_{3+}+s_{4+})}{i(\omega-\omega_R)+\frac{1}{\tau_{0R}}+\frac{1}{\tau_{eR}}} & (10) \end{cases}.$$

Substitute equation (9) into equation (4):

$$s_{2-} = \frac{i(\omega-\omega_A)+\frac{1}{\tau_{0A}}}{i(\omega-\omega_A)+\frac{1}{\tau_{0A}}+\frac{1}{\tau_{eA}}} s_{1+} - \frac{\frac{1}{\tau_{eA}}}{i(\omega-\omega_A)+\frac{1}{\tau_{0A}}+\frac{1}{\tau_{eA}}} s_{2+}. \quad (11)$$

Similarly, substitute equation (10) into equation (5) and (6), respectively:

$$\begin{cases} s_{3-} = \frac{-\frac{1}{\tau_{eR}}}{i(\omega-\omega_R)+\frac{1}{\tau_{0R}}+\frac{1}{\tau_{eR}}} s_{3+} & (12) \\ s_{3-} = \frac{-\frac{1}{\tau_{eR}}}{\mathrm{i}(\omega-\omega_R)+\frac{1}{\tau_{0R}}} s_{4-} & (13) \end{cases}.$$

For simplicity, we define $A = \mathrm{i}(\omega-\omega_A)+\frac{1}{\tau_{0A}}+\frac{1}{\tau_{eA}}$ and $R = \mathrm{i}(\omega-\omega_R)+\frac{1}{\tau_{0R}}+\frac{1}{\tau_{eR}}$. So equation (12) and (13) transform to:

$$\begin{cases} s_{3+} = \frac{R}{-\frac{1}{\tau_{eR}}} s_{3-} & (14) \\ s_{3-} = \frac{-\frac{1}{\tau_{eR}}}{R-\frac{1}{\tau_{eR}}} s_{4-} & (15) \end{cases}.$$

Substitute equation (7), (8), (14) and (15) into equation (11), and with some derivation, we can obtain the transmission coefficient t as:

$$t = \frac{s_{4-}}{s_{1+}} = \frac{\left(A-\frac{1}{\tau_{eA}}\right)\left(R-\frac{1}{\tau_{eR}}\right)}{ARe^{ikl}-\frac{1}{\tau_{eA}}\frac{1}{\tau_{eR}}e^{-ikl}} \quad (16).$$

With similar derivation steps, the reflection coefficient r can be obtained as:

$$r = \frac{-\left(A-\frac{1}{\tau_{eA}}\right)^2\frac{1}{\tau_{eR}}e^{-ikl}}{A(ARe^{ikl}-\frac{1}{\tau_{eA}}\frac{1}{\tau_{eR}}e^{-ikl})} - \frac{\frac{1}{\tau_{eA}}}{A} \quad (17).$$

The absorption can be obtained by $A = 1 - |r|^2 - |t|^2$. The TCMT formalism enables precise description of the acoustic performance of the two HR combination with different intrinsic loss and leakage rate. The parameters can be numerically determined. In a two-port system, the maximum absorption A of a single resonator can only reach 50% [37]. With reflector involved, asymmetric perfect absorption can be achieved since the combination allows the radiated wave from the resonator to be cancelled by the reflected wave from reflector. A quarter-wavelength distance ($L = \lambda/4$) of placement is required for the phase inversion of the reflected wave. Therefore, two annular HR combination is employed and side-coupled to the duct. As shown in Figure 1, the annular HRs are installed to the side of the duct to avoid interfering with the ventilation. The length and width of the HR cavity and neck are denoted as w, h, a and b respectively. The diameter of the duct is defined as $D = 100mm$. The distance between the two HRs is denoted as L. Porous material is inserted into the upstream HR cavity to increase its intrinsic loss, whilst the downstream one is kept empty for the purpose of achieving high reflection.

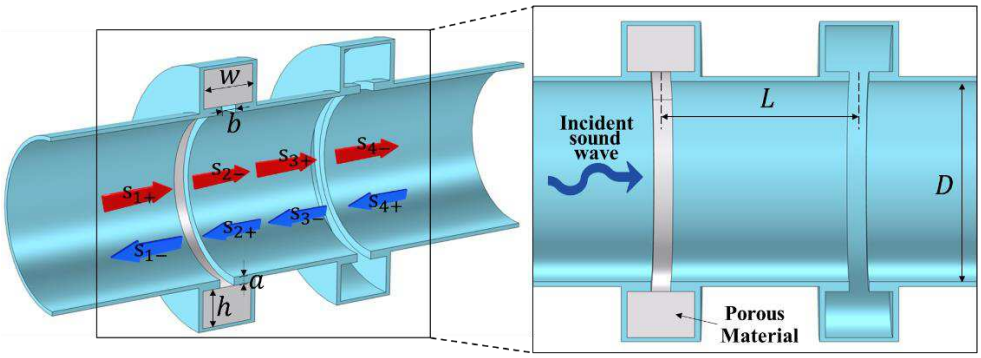

Figure 1. Schematic figure of a duct system side-coupled with double HRs. The double annular HRs are installed to a duct with sound wave incident from one side. The upstream resonator close to the sound incident side is stuffed with porous material.

A numerical simulation technique can be utilized for assisting the design of satisfying critical coupling. By calculating the eigenfrequency with COMSOL Multiphysics, complex eigenfrequency of the HR structure can be obtained as $\omega = \omega_r + j\omega_i$. With proper physical field setting, the imaginary part of the eigenfrequency $|\omega_i|$ of the structure indicates the intrinsic loss γ (mainly caused by friction in HR neck) and leakage rate μ (the wave energy radiating from the resonator), which means the total energy rate of leaking and consuming by the HR. In the numerical model, when only the pressure acoustic physic field is applied, the intrinsic loss caused by friction in HR structure is not included in the model, so $\gamma = 0$ and the imaginary part $\omega_{ilossless}$ solely indicates the leakage rate μ of the structure. Furthermore, when the thermo-viscous acoustics condition is applied to the neck area of the HR, the HR becomes lossy and the imaginary part ω_{ilossy} represents both intrinsic loss and leakage rate. For a reflector, whose intrinsic loss is relatively small, so $\omega_{ilossless} \approx \omega_{ilossy}$ should be fulfilled. Then to simulate the absorber with porous material insertion, the porous material media condition is applied to the cavity domain in the numerical model. The corresponding

imaginary part $\omega_{ilossy+porous}$ will be larger than ω_{ilossy}, with the increment caused by intrinsic loss introduced by the porous material domain. In other words, the critical coupling condition is fulfilled when $\omega_{ilossy} \approx \frac{1}{2}\omega_{iporous}$. Therefore, by combing the absorber and reflector, a duct muffler with asymmetric loss is realized.

Results and discussion

Numerical simulation and analytical modelling are conducted to verify the acoustic performance of the designed muffler structure. Since the geometrical dimension is closely related with the acoustic performance, three sets of HR geometrical parameters, which leads to relatively high reflection capability, are selected, targeting at 3 different frequencies respectively. Numerical simulation model is constructed by the 2D symmetric model in COMSOL Multiphysics. In the model, the mesh size is defined to ensure there are at least 6 elements in the smallest wavelength. The detailed parameters of the HRs and the corresponding eigenfrequencies under various physical field setting in COMSOL Multiphysics are presented in Table 1.

Table 1. Design parameters of the HR targeting different frequencies.

	w	h	a	b	D	D'	Lossless (Hz)	Lossy (Hz)	Porous (Hz)
HR1	15	40	3	5	74	96	1176.2+226.7i	1127.9+239.9i	900.7+365.4i
HR2	25	40	3	5	91	116	940.9+251.6i	897.6+264.2i	731.2+711.0i
HR3	40	40	3	5	116	137	740.57+263.0i	708.5+253.4i	625.4+503.8i

To simplify the design process, the neck length *a* and width *b* are kept unchanged. The constant parameter setting will lead to a relatively stable bandwidth whilst adjusting the HR operation frequencies [23]. The width of the cavity are defined differently for the purpose of adjusting resonant frequencies of the HR structure. As shown in the table, the eigenfrequencies satisfied the condition: $\omega_{ilosslessless} \approx \omega_{ilossy} \approx \frac{1}{2}\omega_{iporous}$. In addition, the distance between the reflector and absorber *D* is defined in accordance with the operation frequency of absorber. The porous material is simulated by utilizing porous media domain with Johnson-Champoux-Allard model[38]. Melamine foam is selected as the filler and the relevant material properties are given in Table 2.

Table 2. Property parameters of the porous material melamine foam [38].

Viscous characteristic length	Thermal characteristic length	Porosity	Flow resistivity	Tortuosity

Melamine foam	213μm	425μm	0.993	13100Pa·sm	1.0053

Firstly, to verify the acoustic performance of single resonators, the numerical calculated acoustic performance spectrum of single HR1-3 absorbers and reflectors side-coupled to duct are compared with the results obtained through analytical model, as given in Figure 2. The analytical curves are obtained through equation (16) and (17). It is observed that the numerical results show good agreement with the analytical calculation results. For HR1, the single absorber (with the parameter $\frac{1}{\tau_{e\_a1}}$=2110, $\frac{1}{\tau_{0\_a1}}$=820 and ω_{0_a1}=890 Hz) can achieve near 50% absorption at the resonant frequencies as denoted in the figure, whilst the reflector ($\frac{1}{\tau_{e\_r1}}$=1410, $\frac{1}{\tau_{0\_r1}}$=105 and ω_{0_r1}=1170 Hz) conducting near total reflection. Because of the insertion of porous material, even though with the same geometry dimension, the absorption frequencies are shifted lower than the corresponding reflection frequencies. Otherwise, the wave dissipation caused by air damping effect leads to the sound absorption in reflectors, and thus hindering the achievement of total reflection. Similar phenomena can also be found for HR2 and HR3. Deviations are found between the analytical and numerical results. Such difference attributes to the assumptions that only the dominant resonant mode is considered in the analytical model, but in the simulation the higher order resonance are also included. Also, coupling of two resonant modes are assumed to be weak and thus neglected in analytical model.

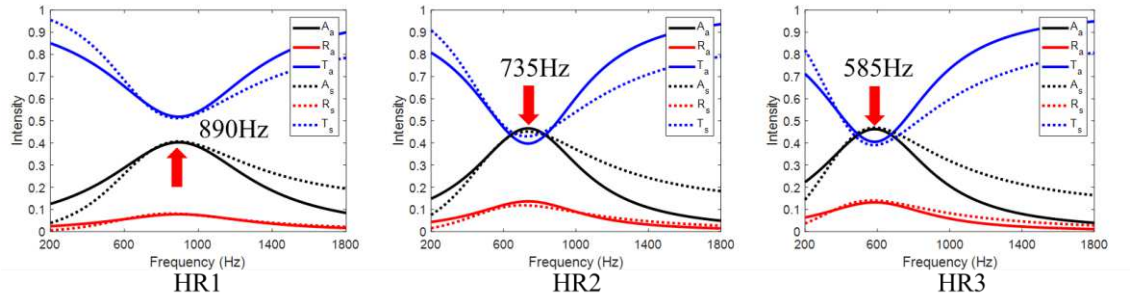

(a)

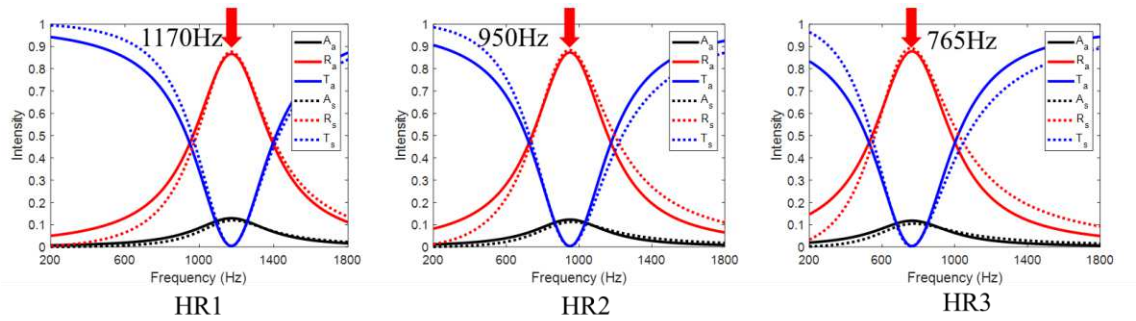

(b)

Figure 2. (a) Acoustic spectrum for HRᵢ performing as absorbers, with the parameters: $\frac{1}{\tau_{e\_ai}}$=820, 850, 850; $\frac{1}{\tau_{0\_ai}}$=2110, 1450, 1490; and ω_{0_ai}=890 Hz, 735Hz, 585Hz; (b) acoustic spectrum for HR1-3 performing as reflectors, with the parameters defined as: $\frac{1}{\tau_{e\_ai}}$=1410,1420,1490; $\frac{1}{\tau_{0\_ai}}$=105,100,100; and ω_{0_ai}=890 Hz, 735Hz, 585Hz. The dashed lines indicate numerical simulation results.

The acoustic performance of the combination of absorber and reflector is then explored experimentally to compare with the simulation and numerical results. Prototypes made by additive manufacturing are fabricated. For each of the prototype, it is designed to consist of 3 parts, by which the annular shape porous material can be inserted into the cavity conveniently. The photograph of the prototype of HR1 is shown in Figure 3(a). The parts are connected by screw bolts and nuts, and melamine foam is chosen as the porous material. Extra testing was conducted to ensure the melamine foam samples have similar property as described in Table 2. The experimental setting is presented in Figure 3(b). The prototype is test through a circular impedance tube (Fantwave F-Tube C). Standard four-microphone method is implemented upon to obtain the transmission, reflection and absorption coefficient. The diameter of the tube is 100mm and the cutoff frequency is about 1800Hz.

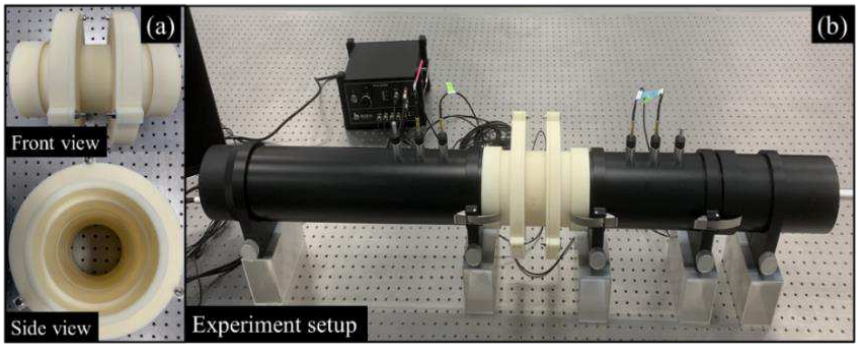

Figure 3.(a) Front and side view photograph of the muffler prototype that manufactured by using the HR1 geometrical parameters. Porous material is cut as cyclic annular and put into the left HR cavity. (b) Experiment setting of the prototype.

For HR1, the measured results are presented in Figure 4(a), compared with the analytical and numerical results. The prototype revealed a maximum absorption of 95.6%, which is slightly larger than 94.6% as predicted in simulation. The designed structure can achieve above 90% absorption in 195Hz width, from about 1122Hz to 1314Hz. The experimental results are mostly consistent with the simulation, except the maximum absorption frequency is about 80Hz higher than simulation. Such deviation mainly attributes to the geometrical error of the sample. The 3D printed epoxy material will slightly shrink after cooling down and will therefore lead to unpredictable geometrical difference. Also, for the analytical model, the corresponding parameters are given as: $\frac{1}{\tau_{e\_a1}}$=820, $\frac{1}{\tau_{0\_a1}}$=2110, $\frac{1}{\tau_{e\_r1}}$=1410, $\frac{1}{\tau_{0\_ri}}$=105. From the parameters, it is obvious that the leakage rate of the reflector is slightly smaller than the intrinsic loss, therefore critical coupling effect is not strictly fulfilled, and PA is only nearly achieved.

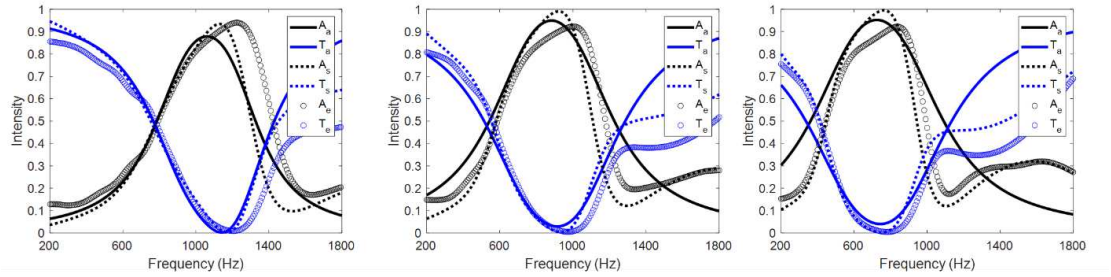

Figure 4. Acoustic spectrum of the muffler form by (a) HR1; (b) HR2; (c) HR3. The analytical (solid line), numerical simulation (dashed line) and experiments (dots) results are presented for comparison.

In addition, the experimental results are also affected by the air damping effect and thus the analytical predicted absorption is relatively lower than measured. The coupling of both resonators has changed the resonance properties, so the parameters of each resonator are different from those firstly investigated in the uncoupled model.

For HR2 and HR3, experimental (simulation) results shown in Figure 4(b) and Figure 4(c), reveal that above 90% absorption can be achieved in the frequency range 920Hz – 1082Hz (790Hz – 1010Hz) and 774Hz – 912Hz (605Hz – 825Hz), respectively. The measured data is about 100Hz higher than the simulation results, yet the tendency and shape of curves are most consistent. The results indicate that the designed muffler structure can provide a near perfect absorption in the desired frequency range. Table 3 gives the detailed analytical parameters and corresponding resonant frequencies of the three HR cases.

Videos that revealing the sound absorption capability of the HR1 in operation frequencies and ventilation status before and after the installation of the mufflers are recorded and given in supplementary material.

Table 3. Analytical parameter of the combined HR pairs.

	$\frac{1}{\tau_{0\_a}}$	$\frac{1}{\tau_{e\_a}}$	$\frac{1}{\tau_{0\_r}}$	$\frac{1}{\tau_{e\_r}}$	ω_a(Hz)	ω_r(Hz)
HR1	1410	450	105	1510	994	1142
HR2	1510	500	550	1550	850	920
HR3	1550	550	110	1510	700	750

We then consider the structure that with lossy resonators on both sides of the reflector unit. The configuration and photograph of the prototype is given in Figure 5(a). Such structure design allows the muffler to conduct sound absorption for wave incident from both sides of the tube and thus brings a better feasibility in actual application. In addition, the usage of extra absorber leads to the increase of absorption bandwidth. The tested results are presented in Figure 5(b). The experimental results are basically consistent with the simulation, except the absorption bandwidth is even broader than predicted. The roughness of the 3D printed sample is not carefully controlled during

the manufacturing process and will therefore bring unexpected friction and broaden the bandwidth.

The measured results indicates that the prototype can conduct above 90% sound absorption in the frequency range 948Hz – 1338Hz (in simulation: 935Hz – 1200Hz). The measured bandwidth is 390Hz, which is about 100% larger than the muffler with only one absorber equipped.

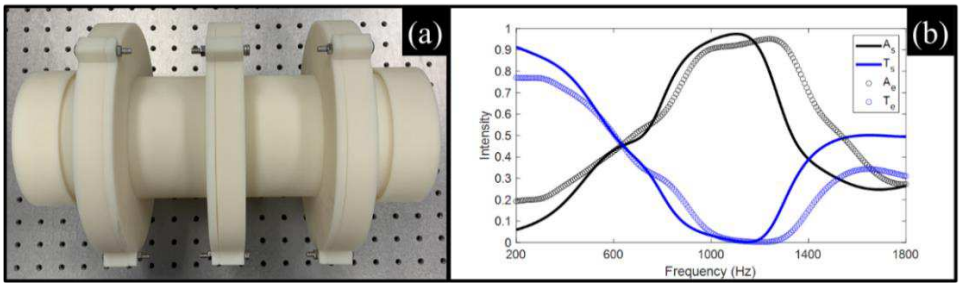

Figure 5. (a) Photograph of the muffler prototype with 3 HR units. The absorbers are allocated on both sides of the reflector HR. (b) Simulation and experiment results of the 3 HR units muffler.

Conclusion

In conclusion, we proposed a muffler design consists of two coupled HR for the sound absorption in two-port ventilation system. The cross section of the circular tube is not transformed after the installation of the designed muffler so to avoid the hindering of ventilation. Analytical model based on TCMT is developed and verified. A convenient numerical method is also introduced for assisting the design of the muffler.

Experimental study was conducted and the results are verified with the analytical and numerical results. The measured results depict that the proposed muffler can achieve near perfect sound absorption in the duct system whilst keeping itself in a subwavelength scale. A symmetry allocation of absorber resonator is also investigated for the purpose of achieving absorbing sound incident from both sides of the ventilation tube. The employment of extra absorber is experimentally proved having a broader sound absorption bandwidth.

We believe such design mechanism and muffler structure provide a promising solution for the sound absorption and noise reduction application in ventilation condition. The absorption operation frequency can be effectively tuned by adjusting the geometrical parameters of the HR structure and thus suitable for different application scenarios.

Reference

1 Kushwaha, M. S., Halevi, P., Dobrzynski, L. & Djafari-Rouhani, B. Acoustic band structure of periodic elastic composites. *Phys Rev Lett* **71**, 2022-2025, doi:10.1103/PhysRevLett.71.2022 (1993).

2 M.Sigalas & E.N.Economou. Band structure of elastic waves in two dimensional systems. *Solid State Communications* **86**, 141-143 (1993).

3 Huang, Y., Li, J., Chen, W. & Bao, R. Tunable bandgaps in soft phononic plates with spring-mass-like resonators. *International Journal of Mechanical Sciences* **151**, 300-313, doi:10.1016/j.ijmecsci.2018.11.029 (2019).

4 Fan, J. *et al.* A review of additive manufacturing of metamaterials and developing trends. *Materials Today* **50**, 303-328 (2021).
5 Cummer, S. A., Christensen, J. & Alù, A. J. N. R. M. Controlling sound with acoustic metamaterials. *Nature Reviews Materials* **1**, 1-13 (2016).
6 Ma, G. & Sheng, P. Acoustic metamaterials: From local resonances to broad horizons. *Science Advances* **2**, e1501595 (2016).
7 Liu, Z. *et al.* Locally resonant sonic materials. *Science* **289**, 1734-1736 (2000).
8 Jimenez, N., Romero-Garcia, V., Pagneux, V. & Groby, J. P. Rainbow-trapping absorbers: Broadband, perfect and asymmetric sound absorption by subwavelength panels for transmission problems. *Sci Rep* **7**, 13595, doi:10.1038/s41598-017-13706-4 (2017).
9 Shao, H., He, H., Chen, Y., Tan, X. & Chen, G. A tunable metamaterial muffler with a membrane structure based on Helmholtz cavities. *Applied Acoustics* **157**, 107022, doi:10.1016/j.apacoust.2019.107022 (2020).
10 Kim, S. R., Kim, Y. H. & Jang, J. H. A theoretical model to predict the low-frequency sound absorption of a Helmholtz resonator array. *The Journal of the Acoustical Society of America* **119**, 1933-1936 (2006).
11 Yang, M., Ma, G., Yang, Z. & Sheng, P. Subwavelength perfect acoustic absorption in membrane-type metamaterials: a geometric perspective. *EPJ Applied Metamaterials* **2**, 10, doi:10.1051/epjam/2015017 (2016).
12 Mei, J. *et al.* Dark acoustic metamaterials as super absorbers for low-frequency sound. *Nat Commun* **3**, 756, doi:10.1038/ncomms1758 (2012).
13 Ma, G., Yang, M., Yang, Z. & Sheng, P. Low-frequency narrow-band acoustic filter with large orifice. *Applied Physics Letters* **103**, 011903, doi:10.1063/1.4812974 (2013).
14 Chen, S. *et al.* Engineering Coiling-Up Space Metasurfaces for Broadband Low-Frequency Acoustic Absorption. *Physica Status Solidi (RRL) – Rapid Research Letters* **13**, 1900426, doi:10.1002/pssr.201900426 (2019).
15 Liu, H., Wu, J. H. & Ma, F. Dynamic tunable acoustic metasurface with continuously perfect sound absorption. *Journal of Physics D: Applied Physics* **54**, 365105 (2021).
16 Li, Y. *et al.* Tunable asymmetric transmission via lossy acoustic metasurfaces. *Physical Review Letters* **119**, 035501 (2017).
17 Zhao, L., Conlon, S. C. & Semperlotti, F. Broadband energy harvesting using acoustic black hole structural tailoring. *Smart Materials and Structures* **23**, 065021, doi:10.1088/0964-1726/23/6/065021 (2014).
18 Gao, N., Wang, B., Lu, K. & Hou, H. Complex band structure and evanescent Bloch wave propagation of periodic nested acoustic black hole phononic structure. *Applied Acoustics* **177**, doi:10.1016/j.apacoust.2020.107906 (2021).
19 Pelat, A., Gautier, F., Conlon, S. C. & Semperlotti, F. The acoustic black hole: A review of theory and applications. *Journal of Sound and Vibration* **476**, 115316, doi:10.1016/j.jsv.2020.115316 (2020).
20 Li, Y. & Assouar, B. M. Acoustic metasurface-based perfect absorber with deep subwavelength thickness. *Applied Physics Letters* **108**, 063502, doi:10.1063/1.4941338 (2016).
21 Merkel, A., Theocharis, G., Richoux, O., Romero-García, V. & Pagneux, V. Control of acoustic absorption in one-dimensional scattering by resonant scatterers. *Applied Physics Letters* **107**, 244102, doi:10.1063/1.4938121 (2015).
22 Wu, X. *et al.* High-efficiency ventilated metamaterial absorber at low frequency. *Applied Physics Letters* **112**, 103505, doi:10.1063/1.5025114 (2018).
23 Lee, T., Nomura, T. & Iizuka, H. Damped resonance for broadband acoustic absorption in one-port and two-port systems. *Scientific Reports* **9**, 13077, doi:10.1038/s41598-019-49222-w (2019).
24 Ma, G., Yang, M., Xiao, S., Yang, Z. & Sheng, P. Acoustic metasurface with hybrid resonances. *Nat Mater* **13**, 873-878, doi:10.1038/nmat3994 (2014).

25 Wei, P., Croënne, C., Tak Chu, S. & Li, J. Symmetrical and anti-symmetrical coherent perfect absorption for acoustic waves. *Applied Physics Letters* **104**, 121902 (2014).
26 Meng, C., Zhang, X., Tang, S. T., Yang, M. & Yang, Z. Acoustic Coherent Perfect Absorbers as Sensitive Null Detectors. *Sci Rep* **7**, 43574, doi:10.1038/srep43574 (2017).
27 Huang, S. *et al.* Acoustic perfect absorbers via spiral metasurfaces with embedded apertures. *Applied Physics Letters* **113**, 233501, doi:10.1063/1.5063289 (2018).
28 Kumar, S. & Lee, H. P. Labyrinthine acoustic metastructures enabling broadband sound absorption and ventilation. *Applied Physics Letters* **116**, 134103, doi:10.1063/5.0004520 (2020).
29 Dong, R. *et al.* Recent advances in acoustic ventilation barriers. *Journal of Physics D: Applied Physics* **54**, 403002, doi:10.1088/1361-6463/ac1228 (2021).
30 Yang, M. *et al.* Subwavelength total acoustic absorption with degenerate resonators. *Applied Physics Letters* **107**, 104104, doi:10.1063/1.4930944 (2015).
31 Xiang, X. *et al.* Ultra-open ventilated metamaterial absorbers for sound-silencing applications in environment with free air flows. *Extreme Mechanics Letters* **39**, 100786 (2020).
32 Long, H., Cheng, Y. & Liu, X. Asymmetric absorber with multiband and broadband for low-frequency sound. *Applied Physics Letters* **111**, 143502, doi:10.1063/1.4998516 (2017).
33 Long, H. *et al.* Tunable and broadband asymmetric sound absorptions with coupling of acoustic bright and dark modes. *Journal of Sound and Vibration* **479**, 115371, doi:10.1016/j.jsv.2020.115371 (2020).
34 Lee, T., Nomura, T., Dede, E. M. & Iizuka, H. J. A. P. L. Asymmetric loss-induced perfect sound absorption in duct silencers. *Applied Physics Letters* **116**, 214101 (2020).
35 C.Manolatou, M.J.Khan, Fan, S., Villeneuve, P. R. & H.A.Haus. Coupling of Modes Analysis of Resonant Channel Add–Drop Filters. *IEEE Journal of Quantum Electronics* **35**, 1322-1331 (1999).
36 Cai, C. & Mak, C. M. Acoustic performance of different Helmholtz resonator array configurations. *Applied Acoustics* **130**, 204-209, doi:10.1016/j.apacoust.2017.09.026 (2018).
37 Yang, M. *et al.* Sound absorption by subwavelength membrane structures: A geometric perspective. *Comptes Rendus Mécanique* **343**, 635-644, doi:10.1016/j.crme.2015.06.008 (2015).
38 Kino, N. Further investigations of empirical improvements to the Johnson–Champoux–Allard model. *Applied Acoustics* **96**, 153-170, doi:10.1016/j.apacoust.2015.03.024 (2015).

Acknowledgement

This research is supported by the Department of Science and Technology of Guangdong Province GDST20SC03 and the Project of Hetao Shenzhen-Hong Kong Science and Technology Innovation Cooperation Zone (HZQB-KCZYB-2020083).

Author Contributions

C.G., C.H., B.H. and W.W. initiated the project; C.G. carried out the analytical derivation, J.M. and Z.D. helped with the analytical model equations; C.H. and X.Z. helped with data analysis and software support; C.G. carried out the numerical simulation and experimental work; W.W. provided funding support; C.G. drafted the initial paper and all authors have equally contributed to the revision.

Data Availability

The data that support the findings of this study are available from the corresponding author upon reasonable request.

Competing interests

The authors declare no competing interests.

Figure legends

Figure 6. Schematic figure of a duct system side-coupled with double HRs. The double annular HRs are installed to a duct with sound wave incident from one side. The upstream resonator close to the sound incident side is stuffed with porous material.

Figure 7. (a) Acoustic spectrum for HR_i performing as absorbers, with the parameters: $\frac{1}{\tau_{e\_ai}}$=820, 850, 850; $\frac{1}{\tau_{0\_ai}}$=2110, 1450, 1490; and ω_{0_ai}=890 Hz, 735Hz, 585Hz; (b) acoustic spectrum for HR1-3 performing as reflectors, with the parameters defined as: $\frac{1}{\tau_{e\_ai}}$=1410,1420,1490; $\frac{1}{\tau_{0\_ai}}$=105,100,100; and ω_{0_ai}=890 Hz, 735Hz, 585Hz. The dashed lines indicate numerical simulation results.

Figure 8.(a) Front and side view photograph of the muffler prototype that manufactured by using the HR1 geometrical parameters. Porous material is cut as cyclic annular and put into the left HR cavity. (b) Experiment setting of the prototype.

Figure 9. Acoustic spectrum of the muffler form by (a) HR1; (b) HR2; (c) HR3. The analytical (solid line), numerical simulation (dashed line) and experiments (dots) results are presented for comparison.

Figure 10. (a) Photograph of the muffler prototype with 3 HR units. The absorbers are allocated on both sides of the reflector HR. (b) Simulation and experiment results of the 3 HR units muffler.

Supplementary Files

This is a list of supplementary files associated with this preprint. Click to download.

- Supplementary.V1.mp4
- Supplementary.V2.mp4